Cell Reports
Physical Science

CellPress
OPEN ACCESS

Report

Nearfield trapping increases lifetime of single-molecule junction by one order of magnitude

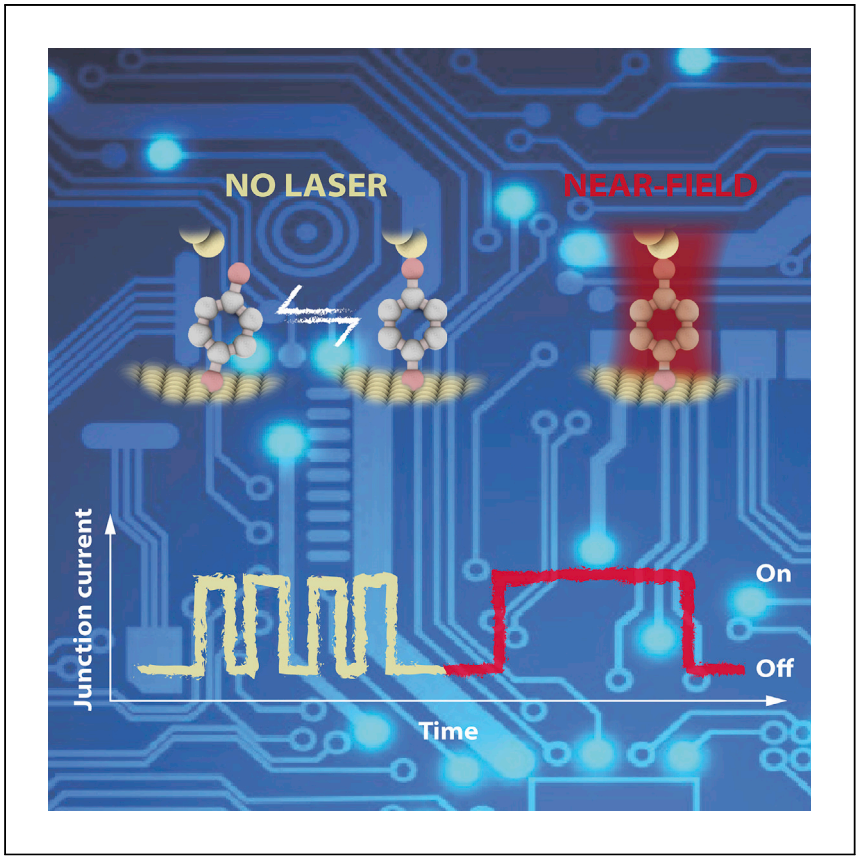

Immobilizing target molecules for seconds or longer interrogation times is one of the main challenges of single-molecule detection platforms. Aragonès and Domke report a plasmon-supported break-junction approach that increases the lifetime of electrically detected molecular junctions by one order of magnitude while maintaining the molecule's native structure and contact geometry.

Albert C. Aragonès, Katrin F. Domke

albert.cortijos@mpip-mainz.mpg.de (A.C.A.)
domke@mpip-mainz.mpg.de (K.F.D.)

HIGHLIGHTS

Nearfield trapping non-invasively increases the lifetime of single-molecule junctions

Moderate far-field power densities (11 mW/μm^2) lead to a >10-fold increase in lifetime

Higher polarizable contact geometries yield larger nearfield trapping efficiencies

Aragonès & Domke, Cell Reports Physical Science *2*, 100389
April 21, 2021
https://doi.org/10.1016/j.xcrp.2021.100389

Please cite this article in press as: Aragonès and Domke, Nearfield trapping increases lifetime of single-molecule junction by one order of magnitude, Cell Reports Physical Science (2021), https://doi.org/10.1016/j.xcrp.2021.100389

Cell Reports
Physical Science

CellPress
OPEN ACCESS

Report

Nearfield trapping increases lifetime of single-molecule junction by one order of magnitude

Albert C. Aragonès[1,*] and Katrin F. Domke[1,2,*]

SUMMARY

Progress in molecular electronics (ME) is largely based on improved understanding of the properties of single molecules (SMs) trapped for seconds or longer to enable their detailed characterization. We present a plasmon-supported break-junction (PBJ) platform to significantly increase the lifetime of SM junctions of 1,4-benzenedithiol (BDT) without the need for chemical modification of molecule or electrode. Moderate far-field power densities of ca. 11 mW/μm^2 lead to a >10-fold increase in minimum lifetime compared with laser-OFF conditions. The nearfield trapping efficiency is twice as large for bridge-site contact compared with hollow-site geometry, which can be attributed to the difference in polarizability. Current measurements and tip-enhanced Raman spectra confirm that native structure and contact geometry of BDT are preserved during the PBJ experiment. By providing a non-invasive pathway to increase short lifetimes of SM junctions, PBJ is a valuable approach for ME, paving the way for improved SM sensing and recognition platforms.

INTRODUCTION

The field of molecular electronics (ME) aims at miniaturizing electronic devices and surpassing the space limitation of conventional silicon circuit integration.[1] In ME, the functionality of the electric circuitry relies on the electronic properties of individual molecules or small molecular ensembles. To improve our understanding of single-molecule electronic properties, ME research fundamentally relies upon the development of novel techniques to reliably and reproducibly study the diverse properties of individual molecules that are inaccessible in conventional ensemble experiments.[2] Robust tools have been developed for high-precision single-molecule trapping and detection to characterize individual molecules, enabling, for example, molecular sensing,[3] recognition,[4] Raman characterization,[5,6] or single-molecule reactors.[7] Most of these approaches rely on the detection of individual molecular binding events in an electrode-electrode gap of a fixed size as a function of time.[4,6–10] One of the most promising approaches to trap and study single molecules bridged in precisely sized, motionless nanogaps is the blinking approach,[11] a scanning tunneling microscope (STM)-based break-junction technique (STM-BJ).[12] In the blinking approach, a subnanometer precise inter-electrode distance is kept between the STM-tip and substrate electrodes to create a molecular-scale metal-metal gap in which an individual target species can be trapped to form a single-molecule electronic junction. When the tunneling current I_t feedback control is disabled, molecular junctions form (and break)[10] stochastically (Figure 1A) in the electrode gap.[13] The formation of a single-molecule junction can be monitored *in situ* by a sudden increase of the measured current signal to the molecular junction current I_m, whose amplitude equals the conductance of the single-molecule junction (Figure 1B).[10] A

[1]Max Planck Institute for Polymer Research, Ackermannweg 10, 55128 Mainz, Germany

[2]Lead contact

*Correspondence: albert.cortijos@mpip-mainz.mpg.de (A.C.A.), domke@mpip-mainz.mpg.de (K.F.D.)

https://doi.org/10.1016/j.xcrp.2021.100389

Please cite this article in press as: Aragonès and Domke, Nearfield trapping increases lifetime of single-molecule junction by one order of magnitude, Cell Reports Physical Science (2021), https://doi.org/10.1016/j.xcrp.2021.100389

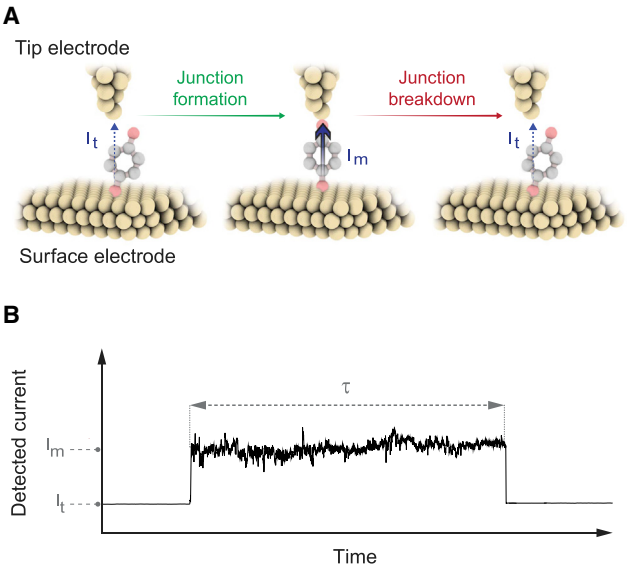

Figure 1. Schematic of the blinking approach for single-molecule junction formation

(A) Left: fixed tip-sample gap distance, no molecular conductive junction, tunneling current I_t. Center: spontaneous formation of the Au-BDT-Au junction with characteristic molecular current I_m. Right: disconnection of the molecule from one electrode and current drop to I_t.

(B) Corresponding detected current response to the sequence depicted in (A). The duration of I_m is the junction lifetime τ.

molecular junction lasts a finite period, i.e., the junction lifetime τ, after which the current suddenly drops again to I_t because of the spontaneous disconnection of the molecule from one of the two electrodes.[11] Typical τ are rather short, on the order of tens to hundreds of milliseconds, thus hindering elaborate junction characterization over longer periods.[6,7,10,14] Immobilizing target molecules for longer timescales, i.e., increasing τ, has remained one of ME's central challenges. Strategies to obtain enduring and mechanically robust molecular junctions include the usage of various electrode materials[3,15,16] and anchoring groups.[17–19] Although these strategies have resulted in improved τ of up to a factor of 2 compared with routinely employed Au-SH or Au-NH_2 electrode-anchoring systems,[16,18] they are typically system specific, which hinders wide applicability to diverse sets of target molecules and electrode materials.

One versatile way to secure particles in a specific location is optical (far-field) trapping. An optical trap is created by tightly focusing a laser beam to generate a strong field gradient in the focal region. This field gradient attracts dielectric particles and directs them to the center of the focus where the field is strongest, reaching typical trapping forces on the order of a few (tens of) piconewtons. Downscaling far-field optical trapping to the single-molecule scale is not straightforward because of the Abbe diffraction limit of approx. λ/2 (λ is the trapping laser wavelength, which for typical applications lies in the visible regime between 500 and 750 nm) of the far-field focus size.[20] Furthermore, the gradient of the optical force becomes weaker with decreasing object size (scaling with the third power of the object size) and results in significantly smaller capturing efficiency and thus a simpler escape from the trap of small objects compared with larger ones.[20,21] Nanophotonics offers a useful nanoscale alternative to conventional optical traps: plasmonic traps.[21] Plasmonic traps are based on nanostructures that confine and enhance an electromagnetic field well beyond the diffraction limit due to (surface) plasmon excitation by

(far-field) light.[20] The resulting nearfield induces strong gradient forces capable of increasing the efficiency and the precision of optical trapping. The intensity of the nearfield can be up to three orders of magnitude stronger than the far-field intensity, rendering feasible even the capture of nanoparticles and molecules, to date down to the 100 to 10 nm range.[22] In recent works, plasmonic trapping was employed to lock dyes and bio-molecules into position at Ag nanoaggregates or Au surfaces for surface-enhanced Raman spectroscopic measurements.[23,24]

Here, we combine nearfield trapping with the blinking STM-BJ approach to enable plasmon-supported break-junction (PBJ) experiments. For the PBJ approach, we integrate an STM-BJ platform[5] into an STM-based solid/liquid tip-enhanced Raman spectrometer (EC-TERS[25]) that allows us to build, stabilize, and characterize well-defined single-molecule junctions *in situ* in terms of τ and other common junction characteristics, such as molecular conductance, junction yield, and adsorption geometry. We form single-molecule junctions of showcase 1,4-benzenedithiol (BDT), a prototypical single-molecule component in ME research that has been shown to interact through one of the terminal −S(H) groups with the Au(111) surface as thiolate,[26] whereas the second thiol group is accessible by the tip[27] to form stable molecular junctions.[28,29] We analyze τ in the presence or absence of a nearfield to assess the stability of the Au-BDT-Au junctions. From the PBJ results in correlation with solid/liquid tip-enhanced Raman (TER) spectra, we find that the presence of a nearfield gradient on the order of 6.3×10^7 V/m leads to a significant increase of τ of the single-molecule junction by up to one order of magnitude. As such, we demonstrate that nearfield trapping provides a straightforward way to increase molecular junction robustness without the need for chemical modification of the target molecule and/or electrode and thus opens new possibilities for single-molecule characterization during prolonged timescales of >1 s without compromising the chemical integrity of the junction.

RESULTS AND DISCUSSION

Assessing the nearfield effects on single-molecule junction characteristics

Figures 2A and 2B shows example telegraphic current traces recorded from Au-BDT-Au junctions of a constant size of 10 Å in water with or without 632.8 nm laser illumination of the junction, i.e., with or without nearfield (technical details in the Supplemental experimental procedures; additional current traces in Figure S1). The telegraphic noise pattern in blinking experiments is associated with thermally activated stochastic junction formation and breaking.[13,14] According to thermodynamic theory,[30] the molecule-tip bond is considered a dynamic state, and the probability of spontaneously breaking down the bond because of thermal fluctuations increases with time (see detailed information, including the S-Au junction-specific case, in Note S1).[30,31] Independent of the illumination setting, the single-molecule junction can be found in one of two discrete conduction states of ca. $2.66 \pm 0.21 \times 10^{-3}$ and $1.10 \pm 0.06 \times 10^{-2}$ G_o, where G_o is the conductance quantum unit of 77.4 μS (1D histogram and 2D maps in Figures S2 and S3). These values are consistent with commonly reported ones in the literature.[28,32–36]

Despite its extensive use in fundamental ME studies, BDT is not a simple system for junction formation. Depending on the experimental approach and employed set-ups, other junction conductance values have been reported, because many processes can lead to a change in the conductance in single-molecule junctions. Electrode pulling was demonstrated to lead to various conductance values for BDT junctions. For example, Bruot et al.[32] observed an increase in junction

Please cite this article in press as: Aragonès and Domke, Nearfield trapping increases lifetime of single-molecule junction by one order of magnitude, Cell Reports Physical Science (2021), https://doi.org/10.1016/j.xcrp.2021.100389

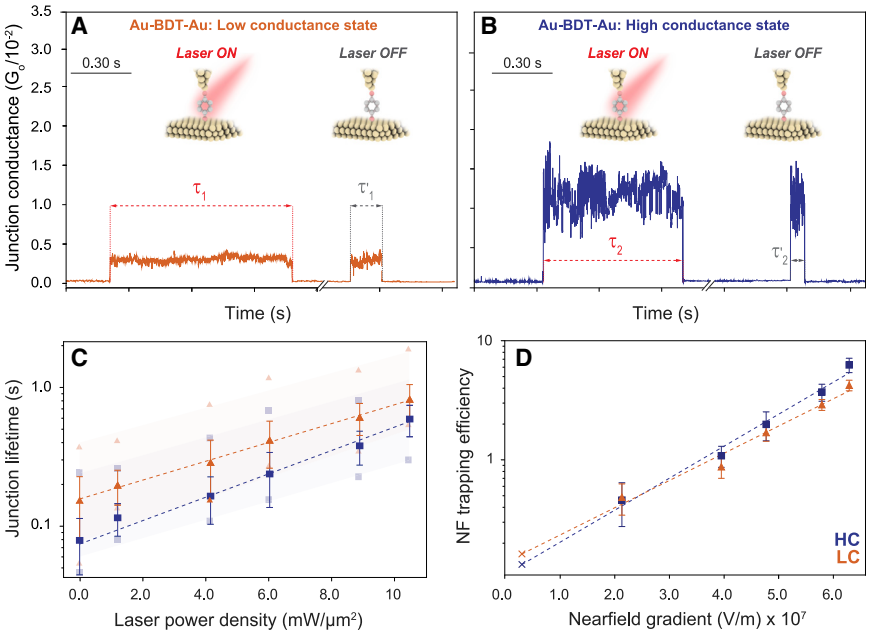

Figure 2. Example of PBJ captures and mean junction lifetime with the nearfield trapping powers under the employed power laser densities

(A and B) Example of PBJ captures of (A) low conductance (LC, orange) and of (B) high conductance (HC, blue) junctions with laser (i.e., nearfield) ON or OFF.

(C) Mean junction lifetime τ as a function of laser power density for LC (orange) and HC (blue) junctions. Shaded areas mark the minimum to maximum 1% distributions (average values marked with bright orange triangles and blue squares, respectively) of all runs.

(D) Calculated nearfield trapping efficiency η as a function of the estimated nearfield gradient for LC (orange) and HC (blue) junctions. The asterisk field gradient corresponds to the bias-induced field. 0 mW control values are an average from all experiments with the laser beam fully blocked. Error bars indicate the dataset standard deviation for each laser power density (C) and nearfield gradient (D) condition.

conductance from 10^{-2} to 10^{-1} G_o because highest occupied molecular orbital (HOMO)-related states shift due to molecule stretching. Similarly, Kim et al.[34] detected BDT junction conductance signatures in a range from ca. 10^{-4} G_o up to close to G_o during junction stretching that they attributed to changes in molecular orientation and contact geometry. Leary et al.[37] reported the detection of low-conducting events at ca. 10^{-4} G_o due to Au-BDT-Au_{adatom}-BDT-Au chain formation because of junction stretching during electrode pulling at high BDT surface coverage. Furthermore, oxidative dimerization of BDT was shown to occur in a break-junction experiment in ambient conditions to form an S-S bridged BDT dimer with a low conductance (LC) signature of ca. 10^{-4} to 10^{-3} G_o,[38] albeit not at low BDT surface coverage.[35] For our experimental conditions, i.e., a fixed tip-sample distance at BDT molecular length, no electrode movement during the PBJ experiments, an oxygen-free environment, and a lower BDT surface coverage compared with the ones in the references cited earlier, these effects can be discarded as explanation for the observed conductance values (details in Note S2).

We thus assign the observed LC and high conductance (HC) states to hollow and bridge BDT-Au adsorption configurations, respectively, as previously associated both experimentally and theoretically.[28,35,36,39] In pulling-based experiments, a BDT-Au atop configuration was also observed by a measured and calculated conductance of ca. 10^{-4} G_o at the maximum inter-electrode distance before junction

collapse.[28,34–36] Because we work in static gap conditions and the observed LC value is one order of magnitude larger than the atop one, we exclude a BDT atop configuration from our experiments.

The corresponding current/voltage (I(V)) characteristics (Note S3; Figure S4) indicate symmetric molecule/electrode contact geometries at both electrodes.[40] Complementary TER spectra (see analysis in Note S4, Figures S5–S7, and Table S1) recorded before and after the PBJ experiments corroborate the presence of intact BDT molecules in the gap through the detection of their characteristic vibrational fingerprint. Furthermore, the stable spectral background provides an independent proof of the gap (plasmonic) stability over the course of a few-hours-long PBJ experiment.

In the absence of the nearfield, the recorded junction mean lifetimes are $\tau_{OFF\text{-}LC}$ = 0.14 ± 0.07 s and $\tau_{OFF\text{-}HC}$ = 0.08 ± 0.03 s for the LC and HC junctions, respectively. HC junctions possess an inherently lower resistance than LC junctions because of the stronger bridge-contact geometry compared with the hollow Au site geometry of LC junctions. The lower resistance negatively affects the HC junction τ because inherent local heating due to stronger electron-phonon interactions lowers the junction stability compared with LC junctions.[41] Interestingly, we observe a drastic increase in mean lifetimes for both LC- and HC-type junctions to $\tau_{ON\text{-}LC}$ = 0.80 ± 0.22 s and $\tau_{ON\text{-}HC}$ = 0.58 ± 0.15 s when the tip-sample gap is illuminated and a nearfield is created. For the highest employed far-field power density of 11 mW/μm^2 (3.3 mW far-field laser power at the diffraction-limited focus spot measured in air; the one in water cannot be measured but is likely to be a factor of 3 to 5 smaller;[42] details in Note S5 and values in Tables S2 and S3), the mean τ increase thus amounts to factors of 6 and 7 for LC and HC junctions, respectively. 1% of the runs show an unprecedented increase in BDT junction lifetime of more than one order of magnitude, i.e., detected HC and LC lifetimes of 1.1 and 1.8 s, respectively. These results demonstrate that creating a nearfield in the tip-sample gap constitutes a highly effective means to stabilize single-molecule junctions already at moderate far-field laser power densities of ca. 11 mW/μm^2. In addition to the increase in τ, we observe an increase in the detected junction yield of up to a factor of 8 between laser OFF and ON conditions, which indicates that the presence of the nearfield facilitates the formation of single-molecule junctions (see Figure S8 and Table S4 and detailed analysis in Note S6). A similar plasmon-supported increase in single-molecule junction probability has been recently reported by Zhan et al.,[43] who were able to tune the capture and release of molecules in a nearfield gap in solution during pulling captures between two electrodes. However, the single-molecule conductance is independent of the absence or presence of the nearfield at the investigated laser powers (see Figure S9 and Table S5 and detailed analysis in Note S7). The electron transmission eigenchannel of BDT is dominated by the HOMO level that is located about 2 eV below the Fermi level of Au.[35] At the 3 mV bias applied here, the overlap of the Au hot-hole energy distribution with the BDT HOMO level is apparently insufficient to create a detectable hot-carrier-induced current.[44]

Figure 2C displays how τ depends on the employed laser power. The data have been extracted from 1D lifetime histograms obtained from hundreds of accumulated PBJ current captures (histograms in Figure S10 and extracted lifetimes in Tables S6–S9) for far-field laser power densities ranging from ca. 1.2 to 11 mW/μm^2 (0.38 to 3.3 mW far-field laser power). For each set of experiments at a specific laser power density, complementary 0 mW/μm^2 *in situ* control experiments were performed by blocking the laser beam (Note S8; Figure S11). The 0 mW/μm^2 data depicted in Figure 2C

Please cite this article in press as: Aragonès and Domke, Nearfield trapping increases lifetime of single-molecule junction by one order of magnitude, Cell Reports Physical Science (2021), https://doi.org/10.1016/j.xcrp.2021.100389

form the mean value of all control experiments. We can fit the laser power dependence of τ to an Arrhenius-like exponential function with degrees of confidence r^2 of 0.997 and 0.987 for the LC and HC traces, respectively:

$$\tau = A \cdot \exp(P / k_B T), \quad \text{(Equation 1)}$$

with A as a constant, P as the incident laser power density, k_B as the Boltzmann constant, and T as the temperature. As such, our single-molecule nearfield trap exhibits a logarithmic increase in τ with employed laser power (density), comparable to the one that has previously been observed for the trapping of large, 100-nm-sized particles in liquid medium in a nanoaperture-based optical trap.[45] The slight difference in the slopes of the LC (0.49) and HC (0.61) traces attests to different susceptibilities of the two types of BDT-Au bonding motifs to the nearfield optical trap. Even though $\tau_{HC} < \tau_{LC}$, apparently the HC state is more strongly stabilized by the presence of the nearfield than the LC state.

To understand the different magnitudes of the nearfield effect on LC and HC junctions, let us consider the physical origin of the lifetime increase. In a plasmonic trap, the emerging gradient force of the nearfield (at a given laser power) acting on the (trapped) species is proportional to the polarizability of the particle or molecule.[46] Observing differences in nearfield trapping efficiencies for LC and HC states therefore points to the two Au-BDT-Au-related adsorption configurations exhibiting different polarizabilities. It has been demonstrated that the conductance of molecules scales with their polarizability.[47] Even more importantly, small differences in molecule-metal contact geometry result in significant changes in polarizability and correlated conductance.[48] In general, the junction polarizability is described by the induced electronic dipolar transition between the frontier orbitals.[49] For Au-BDT, this transition is largely dominated by the HOMO-lowest unoccupied molecular orbital (LUMO) gap that, in turn, depends on the contact geometry.[39] Accordingly, we find the HC Au-BDT-Au state exhibits larger susceptibility to the nearfield than the LC state, which can be associated with the higher polarizability of the HC state compared with the LC state.

To exclude additional parameters inherent to the system that potentially affect τ, such as intrinsic lifetime differences between LC and HC junctions due to current-induced local heating or lifetime variance between sets of experiments under equivalent conditions, and thus to isolate and more precisely quantify the effect of the plasmonic nearfield on τ, we calculate a normalized nearfield trapping efficiency η for each junction. Here, $\eta = (\tau_P - \tau_{OFF} / \tau_{OFF})$, with τ_P as the lifetime under laser illumination at a specific incident laser power density and $\tau_{OFF\text{-}P}$ as the lifetime measured under identical conditions with the laser beam blocked. Furthermore, we convert the employed power density P to an approximate far-field strength E following a $p = E^2/Z_0$ conversion,[50] where Z_0 is the characteristic impedance of free space, and then calculate an approximate nearfield gradient by assuming an enhancement of a factor of 30, which is typical for the given TERS Au-Au gap (Tables S2 and S3).[42]

Figure 2D shows how η increases exponentially with the increasing nearfield gradient for LC junctions, from ca. 0.47 to 6.3 with a slope of 2.9×10^{-8} at a degree of confidence of 0.972, and for HC junctions, from ca. 0.44 to 4.2 with a slope of 3.4×10^{-8} at a degree of confidence of 0.984. Except for the lowest laser power conditions employed here, HC junctions display higher nearfield trapping efficiency values than LC junctions, reaching a nearfield susceptibility that is twice as high at 6.3×10^7 V/m. The differences in slope and η values again indicate a correlation

between the nearfield trapping efficiency and the contact geometry, i.e., the distinctive feature between LC and HC junctions.

When the laser is OFF (no nearfield), a small electric field of ca. 3.0×10^6 V/m still in the gap is associated with the applied bias voltage of 3 mV (cross marker data in Figure 2D).[7] This bias-related field is present during all experiments and can thus be viewed as an offset to the applied nearfield. Fitting the OFF data points with the ON data points, we obtain estimations for the bias-induced contribution to η of 0.13 and 0.16 for LC and HC junctions, respectively. In our experiments, the bias contribution to the stabilization of the junction is thus at least one order of magnitude smaller than the nearfield contribution. In principle, one could increase the bias voltage to create stronger field gradients and thus more stable junctions. However, large biases always imply higher currents and thus greater instabilities of the junctions because of increased electron-phonon interactions.[41] These instabilities could lead to a net decrease of τ, as has been reported for single-protein trapping in plasmonic nanopores.[51]

Nearfield trapping and junction breakdown behavior

How can we understand the blinking lifetime increase of the Au-BDT-Au junction in the presence of a nearfield? First, we need to assess the capability of the employed incident power densities (1.2 to 11 mW/μm^2) to trap individual BDT molecules. Early works by Novotny et al.[46] and Xu and Käll[49] described the theoretical possibility to trap individual molecules in nearfield traps with power densities as small as 1.0 mW/μm^2 and three orders of magnitude of field enhancement, i.e., conditions similar to the ones we employ here.[42] In a recent publication, Long et al.[52] theoretically predicted the plasmon-based trapping effects of individual molecules in an illuminated STM (TERS) nanogap. According to their results, the highly localized electric nearfield creates a radial (restoring) force on the order of 10^{-4} pN/(mW/μm^2) in the nanosized region in the tip-sample gap that is sufficiently strong to orient and stabilize a molecule in the junction. Long et al.[52] used a PBJ tip-sample nanogap geometry of 2 nm, a 60° excitation geometry, a factor of 500 of field intensity enhancement, and a molecule polarizability α of 4.5 Cm^2/V. These conditions are comparable to our system with 1 nm gap size, side-illumination geometry, a field intensity enhancement of 2 to 3 orders of magnitude,[42] and $\alpha_{BDT} = 4.1 \times 10^{-39}$ Cm^2/V (obtained from the Clausius-Mossotti equation; see Supplemental experimental procedures). As such, we conclude that under the given experimental conditions, the generated nearfield optical trapping force in our PBJ experiments is sufficient to direct the BDT molecule toward the center of the illuminated nanogap and trap it there, increasing the junction lifetime.

In the absence of external forces or fields and at low bias voltage regimes of <100 mV,[31] τ exhibits spontaneous junction breakdown behavior following the thermodynamic theory,[30]

$$\tau = t_d \cdot \exp(E_b / k_B T), \qquad \text{(Equation 2)}$$

with t_d as the diffusion time inherent to the system and E_b as the Au-BDT dissociation energy barrier (details in Note S1). When E_b is modified by an external parameter, such as a mechanical force, τ will be affected accordingly.[30] For example, a pulling force from electrode retraction has previously been shown to decrease E_b and thus τ.[31] As evident from comparing Equations 1 and 2, E_b can be understood to be a function of P. We can then separate E_b into field-independent (E_{ind}) and field-dependent (E_{field}) terms as the field contribution that modifies τ according to the field gradient:

$$\tau = t_d \cdot \exp\left([E_{ind} + E_{field}] / k_B T\right), \qquad \text{(Equation 3)}$$

$$\tau = t_d \cdot \exp\left[(E_{ind} / k_B T) + (E_{field} / k_B T)\right],$$

$$\tau = t_d \cdot \exp\left(E_{ind} / k_B T\right) \cdot \exp\left(E_{field} / k_B T\right).$$

With Equation 3, the increase in τ can be estimated from the field gradient values for a given power density P (Table S3). For the maximum P of 11 mW/μm^2, the calculated nearfield gradient equals ca. 6.3 × 10^7 V/m (or 2.2 k_BT/nm), a value comparable to a previously estimated one of ca. 6 k_BT optical potential, resulting from excitation power of tens of milliwatts per square micrometer.[49] In other words, the nearfield associated with the maximum P employed here leads to an increase in the Au-BDT dissociation barrier by 2.2 k_BT. For the lowest power density, Equation 3 yields ca. 2.1 × 10^7 V/m (or 0.80 k_BT/nm), and for the 0 mW/μm^2 control, the small electric field of 3 × 10^6 V/m corresponds to 0.12 k_BT/nm. According to Equation 3, we should thus expect an increase in τ by factors of 2 and 8 for the minimum and maximum power laser densities employed here, respectively, compared with the 0 mW/μm^2 case. Despite the given approximation in field enhancement, the calculated values agree quantitatively well with the experimentally observed ones for HC and LC junctions of 2 and <2 and of 7 and 5, respectively. The stabilizing effect of the nearfield can be expected to break down at some point when heating effects—contributing to the destabilization of the junction—in the gap become non-negligible. For TERS configurations with field enhancements on the order of 20 to 30, comparable to ours, the local temperature rise has been estimated to lie below 10 K.[53] This temperature increase is likely insufficient to promote Au-S desorption[54] or Au-Au fracture.[55] It has been estimated that instabilities of thiol-Au junctions may be relevant above a temperature T increase of 30 K.[56] However, even at these elevated temperatures, blinking experiments did not show signs of a lifetime decrease for Au-S-based molecular junctions.[57]

To corroborate that the nearfield is the driving force for the increased lifetime of single-molecule junctions, two additional types of experiments were performed beside the 0 mW/μm^2 controls. To deliberately suppress or switch off the nearfield trapping in the hotspot region (experimental details in Note S9), we defocus the laser in a controlled way or block the laser immediately after a set of experiments (Figures S12 and S13). The first additional control allows us to exclude far-field effects related to laser illumination, like photocurrent[41] or photothermal effects,[58] that could influence the conductance and the stability of the single-molecule junction. However, turning off the laser immediately after a power-dependent experiment allows us to confirm the reversibility of the plasmon-supported enhancement of τ. Both controls give the same result, namely, that τ is reduced to the original (0 mW/μm^2) value in the absence of a nearfield, confirming that the nearfield is responsible for the observed lifetime increase under focused illumination.

Lifetime and conductance distributions under nearfield

To provide a more in-depth lifetime characterization in the presence of the nearfield, we plot 2D τ versus conductance-distribution maps for the PBJ current captures as a function of applied laser power density (Figure 3). The 2D maps allow us to visualize the τ-distribution envelope and extract the mean lifetimes, as well as to directly correlate them to the conductance-distribution envelope for each power density (detailed description in Note S8). Figure 3 visualizes the transition from τ_{LC} = 0.20 ± 0.06 s and τ_{HC} = 0.11 ± 0.03 s at 1.2 mW/μm^2 power density to

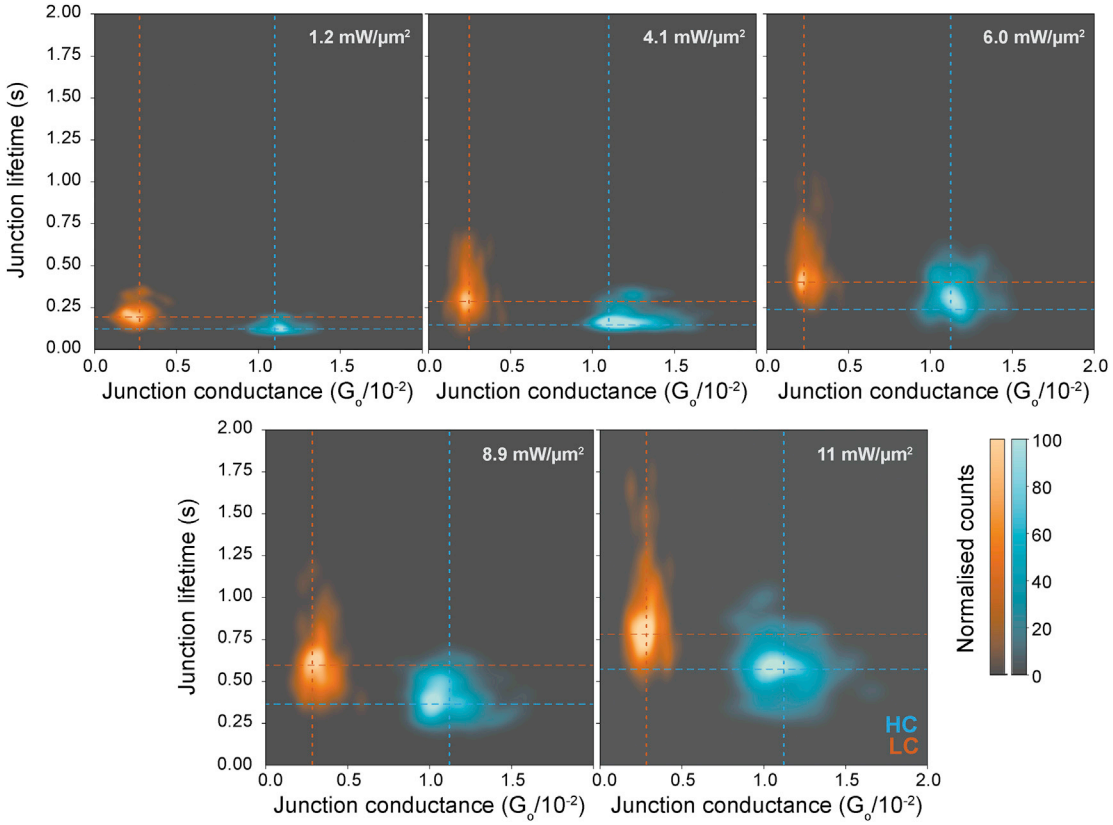

Figure 3. Junction lifetime 2D distribution maps for the employed power laser densities

HC (blue) and LC (orange) 2D distribution maps of junction lifetime τ as a function of junction conductance for the indicated power laser densities in each panel. Counts (number of datapoints with a given lifetime-conductance relation) are normalized to the total number of processed captures to have equivalent ranges of counts (and color scales) between sets of experiments.

τ_{LC} = 0.80 ± 0.22 s and τ_{LC} = 0.58 ± 0.15 s at 11 mW/μm^2 power density (horizontal lines). From the 2D maps, it is evident that the conductance values (envelopes) are independent of the τ distributions at any given power density, with the mean τ regions corresponding to the mean conductance values (cf. 1D histograms in Figure S2). This observation proves that the τ increase is not related to structural modification of the molecule or a contact alteration, because such geometric changes would lead to changes in conductance.[28,35,36] Because we only observe conductance values assigned to single-molecule junctions (not integer multiples of these values), multi-molecule contacts can also be ruled out. Such an assessment of individual molecular contacts is relevant for a τ analysis in plasmonic traps, because multi-molecule cooperative effects have been reported to affect the trapping time.[51,59]

The spatial distribution of the 2D envelopes around the mean τ values contains information about how τ evolves with the laser power density. Interestingly, both minimum and maximum envelope τ values are displaced to higher values with increasing nearfield strength (overview in Table S8). For LC junctions, we observe an increase of the largest 1% τ values (<10 junctions) by a factor of ca. 7 and of the shortest 1% τ values by a factor of 11 compared with the 0 mW/μm^2 values. For HC junctions, we observe an increase of the largest 1% τ values by a factor of ca. 5 and of the shortest 1% τ values by a factor of 5 compared with the 0 mW/μm^2 values. As such, the presence of the nearfield tunes both lower and higher τ thresholds but does so in

Please cite this article in press as: Aragonès and Domke, Nearfield trapping increases lifetime of single-molecule junction by one order of magnitude, Cell Reports Physical Science (2021), https://doi.org/10.1016/j.xcrp.2021.100389

a non-uniform way. The asymmetric τ increase is corroborated by the enlargement of the standard deviation and the area of lifetime histograms as fitted by a gamma distribution commonly used in skewed distributions like the one of blinking junction lifetimes.[57] Because the histograms are normalized to the maximum number of counts, we can quantify the dispersion of the lifetime values by comparing the area ratios. The increase in dispersion as determined from the gamma fitting reaches up to a factor of 5, with areas of 0.389 and 0.359 at 11 mW/μm^2 compared with 0.085 and 0.073 at 0 mW/μm^2 for LC and HC junctions, respectively (Table S9). We can potentially attribute the broadening of the τ distributions to two effects, namely, to the longer lifetime and/or to an increase of heating effects causing small structural variations in the junction. As stated earlier, heating effects should be negligible under the given conditions. Interestingly, Tsutsui et al.[60] reported a correlation between lifetime values and their dispersion for metallic junctions that the authors related to an increase of E_b with increasing lifetime. According to our calculations, E_b increases with laser power density (see Discussion). As such, we attribute the observed increase in lifetime distribution to the longer lifetimes caused by the increase in E_b with increasing laser power.

In any case, we stress that despite the broadening, the entire τ distribution is displaced to larger values in the presence of the nearfield. The result, that less stable junctions are stabilized to a larger extent than more stable junctions, may be of relevance for ME applications, in which the minimum junction lifetime is a limiting factor for junction screening or device applications for sensing and recognition.

Figures 3 and S9, as well as Table S5, also show that the conductance value dispersion (around the stable conductance mean value) increases with lifetime (i.e., laser power). We speculate that this dispersion increase in conductance (i.e., increase in current fluctuation) is related to the enhanced probability to capture molecular processes with slow kinetics and enlarged detection timescales. One known example for a slow kinetic process that yields current fluctuations is Au atomic motion. In a previous single-molecule study, current captures showed higher fluctuations when the junction lifetime was increased by reducing the electrode pulling rate to a value comparable to the Au surface diffusion speed (0.02–0.003 nm/s at room temperature).[61] In earlier work, Xiang et al.[62] found an exponential correlation between the bias voltage and the current fluctuations. The authors ascribed the observations to Au atomic motion on the electrode that is thermally activated by the current intensity, as driven by the applied bias voltage. In addition, optical irradiation was shown to affect the surface dynamics of Au atoms.[63] In our work, the generally slow Au atomic motion and the fluctuations in conductance related to it should thus be detectable during long junction lifetimes. In addition, the presence of the optical nearfield likely promotes Au atomic motion and, as a consequence, current fluctuations.

In summary, with PBJ, we present a combined STM-BJ and EC-TERS platform to investigate how a gap nearfield can be exploited to strengthen spontaneously formed single-molecule junctions. PBJ experiments on Au-BDT-Au junctions are shown to efficiently increase the junction lifetime without the need for chemical modification of molecule and/or electrode. The nearfield is employed to overcome the native stochastic disconnection of the junction, imposing a deterministic lifetime. We quantify experimentally and theoretically how the presence of a nearfield increases the junction lifetime exponentially because of the mechanical stabilization of BDT in the Au-Au gap with the help of an optical gradient force. A moderate far-field power density of ca. 11 mW/μm^2 is found to lead to an effective increase in the

junction dissociation barrier by about 2.2 k_BT. For the given experimental parameters, we achieve an average increase in lifetime by a factor of 7, increasing the lifetimes of hundreds of junctions from hundreds of milliseconds to the order of seconds, reaching values up to 1.8 s. The detected minimum lifetimes increase by more than one order of magnitude. The nearfield trap affects the two observed contact geometries differently, i.e., LC hollow and HC bridge geometry. HC junctions are up to twice as susceptible to nearfield trapping as LC junctions. This difference can be attributed to the larger polarizability of HC junctions compared with LC ones. The development of PBJ represents a significant contribution to the ME field by implementing plasmonic trapping to increase the lifetime of a single-molecule junction while preserving the target molecule's native structure and contact geometry. Our findings can benefit the range of existing fixed-gap molecular platforms on which short lifetimes are often the main bottleneck limiting practical applicability, such as sensing and recognition.

EXPERIMENTAL PROCEDURES

Resource availability

Lead contact

Further information and requests for resources and reagents should be directed to and will be fulfilled by the lead contact, Katrin F. Domke (domke@mpip-mainz.mpg.de).

Materials availability

This study did not generate new unique materials.

Data and code availability

All data, treatment code, and additional information supporting the findings of this study are available from the corresponding authors upon reasonable request.

General procedures

Full descriptions of all single-molecule conductance measurements and data treatment details can be found in the Supplemental experimental procedures.

SUPPLEMENTAL INFORMATION

Supplemental information can be found online at https://doi.org/10.1016/j.xcrp.2021.100389.

ACKNOWLEDGMENTS

A.C.A. thanks the European Union for a H2020-MSCA-IF-2018 Fellowship (TEChMoDE, 844668). K.F.D. is grateful for generous funding through the Plus 3 program of the Boehringer Ingelheim Foundation.

AUTHOR CONTRIBUTIONS

Conceptualization, A.C.A.; methodology, A.C.A.; software, A.C.A.; validation, A.C.A.; formal analysis, A.C.A. and K.F.D.; investigation, A.C.A.; resources, A.C.A. and K.F.D.; data curation, A.C.A. and K.F.D.; writing – original draft preparation, A.C.A. and K.F.D.; writing – review and editing, A.C.A. and K.F.D.; visualization, A.C.A.; supervision, A.C.A. and K.F.D.; project administration, A.C.A.; funding acquisition, K.F.D. and A.C.A. Both authors have read and agreed to the published version of the manuscript.

DECLARATION OF INTERESTS

The authors declare no competing interests.

Received: December 5, 2020
Revised: February 17, 2021
Accepted: March 9, 2021
Published: March 26, 2021

REFERENCES

1. Moore, G.E. (1998). Cramming more components onto integrated circuits. Proc. IEEE *86*, 82–85.

2. Chen, F., Hihath, J., Huang, Z., Li, X., and Tao, N.J. (2007). Measurement of single-molecule conductance. Annu. Rev. Phys. Chem. *58*, 535–564.

3. Guo, X. (2013). Single-molecule electrical biosensors based on single-walled carbon nanotubes. Adv. Mater. *25*, 3397–3408.

4. Chang, S., Huang, S., He, J., Liang, F., Zhang, P., Li, S., Chen, X., Sankey, O., and Lindsay, S. (2010). Electronic signatures of all four DNA nucleosides in a tunneling gap. Nano Lett. *10*, 1070–1075.

5. Liu, Z., Ding, S.-Y., Chen, Z.-B., Wang, X., Tian, J.-H., Anema, J.R., Zhou, X.-S., Wu, D.-Y., Mao, B.-W., Xu, X., et al. (2011). Revealing the molecular structure of single-molecule junctions in different conductance states by fishing-mode tip-enhanced Raman spectroscopy. Nat. Commun. *2*, 305.

6. Jeong, H., Li, H.B., Domulevicz, L., and Hihath, J. (2020). An On-Chip Break Junction System for Combined Single-Molecule Conductance and Raman Spectroscopies. Adv. Funct. Mater. *30*, 2000615.

7. Aragonès, A.C., Haworth, N.L., Darwish, N., Ciampi, S., Bloomfield, N.J., Wallace, G.G., Diez-Perez, I., and Coote, M.L. (2016). Electrostatic catalysis of a Diels-Alder reaction. Nature *531*, 88–91.

8. Brunner, J., González, M.T., Schönenberger, C., and Calame, M. (2014). Random telegraph signals in molecular junctions. J. Phys. Condens. Matter *26*, 474202.

9. Jia, C., Migliore, A., Xin, N., Huang, S., Wang, J., Yang, Q., Wang, S., Chen, H., Wang, D., Feng, B., et al. (2016). Covalently bonded single-molecule junctions with stable and reversible photoswitched conductivity. Science *352*, 1443–1445.

10. Haiss, W., Nichols, R.J., van Zalinge, H., Higgins, S.J., Bethell, D., and Schiffrin, D.J. (2004). Measurement of single molecule conductivity using the spontaneous formation of molecular wires. Phys. Chem. Chem. Phys. *6*, 4330–4337.

11. Aragonès, A.C., Darwish, N., Saletra, W.J., Pérez-García, L., Sanz, F., Puigmartí-Luis, J., Amabilino, D.B., and Díez-Pérez, I. (2014). Highly conductive single-molecule wires with controlled orientation by coordination of metalloporphyrins. Nano Lett. *14*, 4751–4756.

12. Xu, B., and Tao, N.J. (2003). Measurement of single-molecule resistance by repeated formation of molecular junctions. Science *301*, 1221–1223.

13. Asar, J.A.O., Mariscal, M.M., and Leiva, E.P.M. (2009). Stochastic model for spontaneous formation of molecular wires. Electrochim. Acta *54*, 2977–2982.

14. Hasegawa, Y., Harashima, T., Jono, Y., Seki, T., Kiguchi, M., and Nishino, T. (2019). Kinetic investigation of a chemical process in single-molecule junction. Chem. Commun. (Camb.) *56*, 309–312.

15. Aragonès, A.C., Aravena, D., Valverde-Muñoz, F.J., Real, J.A., Sanz, F., Díez-Pérez, I., and Ruiz, E. (2017). Metal-Controlled Magnetoresistance at Room Temperature in Single-Molecule Devices. J. Am. Chem. Soc. *139*, 5768–5778.

16. Aragonès, A.C., Darwish, N., Ciampi, S., Sanz, F., Gooding, J.J., and Díez-Pérez, I. (2017). Single-molecule electrical contacts on silicon electrodes under ambient conditions. Nat. Commun. *8*, 15056.

17. Hong, W., Li, H., Liu, S.X., Fu, Y., Li, J., Kaliginedi, V., Decurtins, S., and Wandlowski, T. (2012). Trimethylsilyl-terminated oligo(phenylene ethynylene)s: an approach to single-molecule junctions with covalent Au-C σ-bonds. J. Am. Chem. Soc. *134*, 19425–19431.

18. Pla-Vilanova, P., Aragonès, A.C., Ciampi, S., Sanz, F., Darwish, N., and Diez-Perez, I. (2015). The spontaneous formation of single-molecule junctions via terminal alkynes. Nanotechnology *26*, 381001.

19. Chen, F., Li, X., Hihath, J., Huang, Z., and Tao, N. (2006). Effect of anchoring groups on single-molecule conductance: comparative study of thiol-, amine-, and carboxylic-acid-terminated molecules. J. Am. Chem. Soc. *128*, 15874–15881.

20. Bouloumis, T.D., and Nic Chormaic, S. (2020). From Far-Field to Near-Field Micro- and Nanoparticle Optical Trapping. Appl. Sci. (Basel) *10*, 1375.

21. Juan, M.L., Righini, M., and Quidant, R. (2011). Plasmon nano-optical tweezers. Nat. Photonics *5*, 349–356.

22. Shoji, T., and Tsuboi, Y. (2014). Plasmonic optical tweezers toward molecular manipulation: Tailoring plasmonic nanostructure, light source, and resonant trapping. J. Phys. Chem. Lett. *5*, 2957–2967.

23. Kitahama, Y., Funaoka, M., and Ozaki, Y. (2019). Plasmon-Enhanced Optical Tweezers for Single Molecules on and near a Colloidal Silver Nanoaggregate. J. Phys. Chem. C *123*, 18001–18006.

24. Huang, J.-A., Mousavi, M.Z., Zhao, Y., Hubarevich, A., Omeis, F., Giovannini, G., Schütte, M., Garoli, D., and De Angelis, F. (2019). SERS discrimination of single DNA bases in single oligonucleotides by electro-plasmonic trapping. Nat. Commun. *10*, 5321.

25. Martín Sabanés, N., and Domke, K.F. (2017). Raman Under Water—Nonlinear and Nearfield Approaches for Electrochemical Surface Science. ChemElectroChem *4*, 1814–1823.

26. Joo, S.W., Han, S.W., and Kim, K. (2001). Adsorption of 1,4-benzenedithiol on gold and silver surfaces: Surface-enhanced Raman scattering study. J. Colloid Interface Sci. *240*, 391–399.

27. Yoshida, S., Taninaka, A., Sugita, Y., Katayama, T., Takeuchi, O., and Shigekawa, H. (2016). Revealing the Conformational Dynamics in a Single-Molecule Junction by Site- and Angle-Resolved Dynamic Probe Method. ACS Nano *10*, 11211–11218.

28. Komoto, Y., Fujii, S., Nakamura, H., Tada, T., Nishino, T., and Kiguchi, M. (2016). Resolving metal-molecule interfaces at single-molecule junctions. Sci. Rep. *6*, 26606.

29. Xiao, X., Xu, B., and Tao, N.J. (2004). Measurement of Single Molecule Conductance: Benzenedithiol and Benzenedimethanethiol. Nano Lett. *4*, 267–271.

30. Evans, E. (2001). Probing the relation between force—lifetime—and chemistry in single molecular bonds. Annu. Rev. Biophys. Biomol. Struct. *30*, 105–128.

31. Huang, Z., Chen, F., Bennett, P.A., and Tao, N. (2007). Single molecule junctions formed via Au-thiol contact: stability and breakdown mechanism. J. Am. Chem. Soc. *129*, 13225–13231.

32. Bruot, C., Hihath, J., and Tao, N. (2011). Mechanically controlled molecular orbital alignment in single molecule junctions. Nat. Nanotechnol. *7*, 35–40.

33. Horiguchi, K., Tsutsui, M., Kurokawa, S., and Sakai, A. (2009). Electron transmission characteristics of Au/1,4-benzenedithiol/Au junctions. Nanotechnology *20*, 025204.

34. Kim, Y., Pietsch, T., Erbe, A., Belzig, W., and Scheer, E. (2011). Benzenedithiol: a broad-range single-channel molecular conductor. Nano Lett. *11*, 3734–3738.

35. Kaneko, S., Montes, E., Suzuki, S., Fujii, S., Nishino, T., Tsukagoshi, K., Ikeda, K., Kano, H.,

Nakamura, H., Vázquez, H., and Kiguchi, M. (2019). Identifying the molecular adsorption site of a single molecule junction through combined Raman and conductance studies. Chem. Sci. (Camb.) *10*, 6261–6269.

36. Kaneko, S., Murai, D., Marqués-González, S., Nakamura, H., Komoto, Y., Fujii, S., Nishino, T., Ikeda, K., Tsukagoshi, K., and Kiguchi, M. (2016). Site-Selection in Single-Molecule Junction for Highly Reproducible Molecular Electronics. J. Am. Chem. Soc. *138*, 1294–1300.

37. Leary, E., Zotti, L.A., Miguel, D., Márquez, I.R., Palomino-Ruiz, L., Cuerva, J.M., Rubio-Bollinger, G., González, M.T., and Agrait, N. (2018). The Role of Oligomeric Gold-Thiolate Units in Single-Molecule Junctions of Thiol-Anchored Molecules. J. Phys. Chem. C *122*, 3211–3218.

38. Zheng, J., Liu, J., Zhuo, Y., Li, R., Jin, X., Yang, Y., Chen, Z.B., Shi, J., Xiao, Z., Hong, W., and Tian, Z.Q. (2018). Electrical and SERS detection of disulfide-mediated dimerization in single-molecule benzene-1,4-dithiol junctions. Chem. Sci. *9*, 5033–5038.

39. Nara, J., Geng, W.T., Kino, H., Kobayashi, N., and Ohno, T. (2004). Theoretical investigation on electron transport through an organic molecule: effect of the contact structure. J. Chem. Phys. *121*, 6485–6492.

40. Briechle, B.M., Kim, Y., Ehrenreich, P., Erbe, A., Sysoiev, D., Huhn, T., Groth, U., and Scheer, E. (2012). Current-voltage characteristics of single-molecule diarylethene junctions measured with adjustable gold electrodes in solution. Beilstein J. Nanotechnol. *3*, 798–808.

41. Huang, Z., Chen, F., D'agosta, R., Bennett, P.A., Di Ventra, M., and Tao, N. (2007). Local ionic and electron heating in single-molecule junctions. Nat. Nanotechnol. *2*, 698–703.

42. Martín Sabanés, N., Driessen, L.M.A., and Domke, K.F. (2016). Versatile Side-Illumination Geometry for Tip-Enhanced Raman Spectroscopy at Solid/Liquid Interfaces. Anal. Chem. *88*, 7108–7114.

43. Zhan, C., Wang, G., Yi, J., Wei, J.-Y., Li, Z.-H., Chen, Z.-B., Shi, J., Yang, Y., Hong, W., and Tian, Z.-Q. (2020). Single-Molecule Plasmonic Optical Trapping. Matter *3*, 1350–1360.

44. Reddy, H., Wang, K., Kudyshev, Z., Zhu, L., Yan, S., Vezzoli, A., Higgins, S.J., Gavini, V., Boltasseva, A., Reddy, P., et al. (2020). Determining plasmonic hot-carrier energy distributions via single-molecule transport measurements. Science *369*, 423–426.

45. Juan, M.L., Gordon, R., Pang, Y., Eftekhari, F., and Quidant, R. (2009). Self-induced back-action optical trapping of dielectric nanoparticles. Nat. Phys. *5*, 915–919.

46. Novotny, L., Bian, R.X., and Xie, X.S. (1997). Theory of Nanometric Optical Tweezers. Phys. Rev. Lett. *79*, 645–648.

47. Cyr, D.M., Venkataraman, B., Flynn, G.W., Black, A., and Whitesides, G.M. (1996). Functional group identification in scanning tunneling microscopy of molecular adsorbates. J. Phys. Chem. *100*, 13747–13759.

48. Moore, A.M., Yeganeh, S., Yao, Y., Claridge, S.A., Tour, J.M., Ratner, M.A., and Weiss, P.S. (2010). Polarizabilities of adsorbed and assembled molecules: measuring the conductance through buried contacts. ACS Nano *4*, 7630–7636.

49. Xu, H., and Käll, M. (2002). Surface-plasmon-enhanced optical forces in silver nanoaggregates. Phys. Rev. Lett. *89*, 246802.

50. Balanis, C. (2016). Antenna Theory: Analysis and Design, Fourth Edition (John Wiley & Sons).

51. Verschueren, D., Shi, X., and Dekker, C. (2019). Nano-Optical Tweezing of Single Proteins in Plasmonic Nanopores. Small Methods *3*, 1800465.

52. Long, L., Chen, J., Yu, H., and Li, Z.-Y. (2020). Strong optical force of a molecule enabled by the plasmonic nanogap hot spot in a tip-enhanced Raman spectroscopy system. Photon. Res. *8*, 1573.

53. Downes, A., Salter, D., and Elfick, A. (2006). Heating effects in tip-enhanced optical microscopy. Opt. Express *14*, 5216–5222.

54. Bürgi, T. (2015). Properties of the gold-sulphur interface: from self-assembled monolayers to clusters. Nanoscale *7*, 15553–15567.

55. Todorov, T.N., Hoekstra, J., and Sutton, A.P. (2001). Current-induced embrittlement of atomic wires. Phys. Rev. Lett. *86*, 3606–3609.

56. Huang, Z., Xu, B., Chen, Y., Di Ventra, M., and Tao, N. (2006). Measurement of current-induced local heating in a single molecule junction. Nano Lett. *6*, 1240–1244.

57. Ruiz, M.P., Aragonès, A.C., Camarero, N., Vilhena, J.G., Ortega, M., Zotti, L.A., Pérez, R., Cuevas, J.C., Gorostiza, P., and Díez-Pérez, I. (2017). Bioengineering a Single-Protein Junction. J. Am. Chem. Soc. *139*, 15337–15346.

58. Wang, K., Meyhofer, E., and Reddy, P. (2020). Thermal and Thermoelectric Properties of Molecular Junctions. Adv. Funct. Mater. *30*, 1904534.

59. Chen, C., Juan, M.L., Li, Y., Maes, G., Borghs, G., Van Dorpe, P., and Quidant, R. (2012). Enhanced optical trapping and arrangement of nano-objects in a plasmonic nanocavity. Nano Lett. *12*, 125–132.

60. Tsutsui, M., Shoji, K., Taniguchi, M., and Kawai, T. (2008). Formation and self-breaking mechanism of stable atom-sized junctions. Nano Lett. *8*, 345–349.

61. Kim, Y.H., Kim, H.S., Lee, J., Tsutsui, M., and Kawai, T. (2017). Stretching-Induced Conductance Variations as Fingerprints of Contact Configurations in Single-Molecule Junctions. J. Am. Chem. Soc. *139*, 8286–8294.

62. Xiang, D., Lee, T., Kim, Y., Mei, T., and Wang, Q. (2014). Origin of discrete current fluctuations in a single molecule junction. Nanoscale *6*, 13396–13401.

63. Carnegie, C., Griffiths, J., de Nijs, B., Readman, C., Chikkaraddy, R., Deacon, W.M., Zhang, Y., Szabó, I., Rosta, E., Aizpurua, J., and Baumberg, J.J. (2018). Room-Temperature Optical Picocavities below 1 nm ^{3} Accessing Single-Atom Geometries. J. Phys. Chem. Lett. *9*, 7146–7151.